Supporting Information for

Corannurylene Pentapetalae

Dong Meng,[†,‡] Guogang Liu,[‡,§] Chengyi Xiao,[⊥] Yanjun Shi,[‡] Lei Zhang,[⊥] Lang Jiang,[‡] Kim K. Baldridge,[#] Yan Li,[*,‡,§] Jay S. Siegel[*,#] and Zhaohui Wang[*,†,‡]

[†]Key Laboratory of Organic Optoelectronics and Molecular Engineering, Department of Chemistry, Tsinghua University, Beijing 100084, China

[‡]Beijing National Laboratory for Molecular Sciences, CAS Key Laboratory of Organic Solids, CAS Center of Excellence in Molecular Science, Institute of Chemistry, Chinese Academy of Sciences, Beijing 100190, China

[#]School of Pharmaceutical Science and Technology, Tianjin University, 92 Weijin Road, Nankai District, Tianjin 300072, China

[⊥]College of Energy, Beijing University of Chemical Technology, Beijing 100029, China

[§]School of Chemistry and Chemical Engineering, University of Chinese Academy of Sciences, Beijing 100049, China

Table of Contents

Materials and Measurements

Perylene-3,4,9,10-tetracarboxylic diimides,1-bromo-perylene-3,4,9,10-tetracarboxylic diimides were synthesized using known procedures.[1] All chemicals and solvents were purchased from commercial suppliers and used without further purification unless otherwise specified.

^{1}H NMR (500 MHz) and ^{13}C NMR (125 MHz) spectra were recorded in deuterated solvents on a Bruker ADVANCE 500 NMR Spectrometer. *J* values are expressed in Hz and quoted chemical shifts are in ppm downfield from tetramethylsilane (TMS) reference using the residual protonated solvent as an internal standard. The signals have been designated as follows: s (singlet), d (doublet), t (triplet), q (quartet), sd (singlet doublet), dd (doublet doublet) and m (multiplets). High resolution mass spectra (HRMS) were determined on IonSpec 4.7 Tesla Fourier Transform Mass Spectrometer.

UV-vis spectra were measured with Hitachi (Model U-3010) UV-vis spectrophotometer in a 1-cm quartz cell. Cyclic voltammograms (CVs) were recorded on a Zahner IM6e electrochemical workstation using glassy carbon discs as the working electrode, Pt wire as the counter electrode, Ag/AgCl electrode as the reference electrode at a scanning rate of 100 mV/s. 0.1 M tetrabutylammoniumhexafluorophosphate (Bu_4NPF_6) dissolved in CH_2Cl_2 was employed as the supporting electrolyte, which was calibrated by the ferrocene/ferroncenium (Fc/Fc^+) as the redox couple. CH_2Cl_2 was freshly distilled prior to use. The microscope images of all the micro-/nano-crystals were acquired by an optical microscope (Vision Engineering Co., UK), which was coupled to a CCD camera.

Synthetic Details

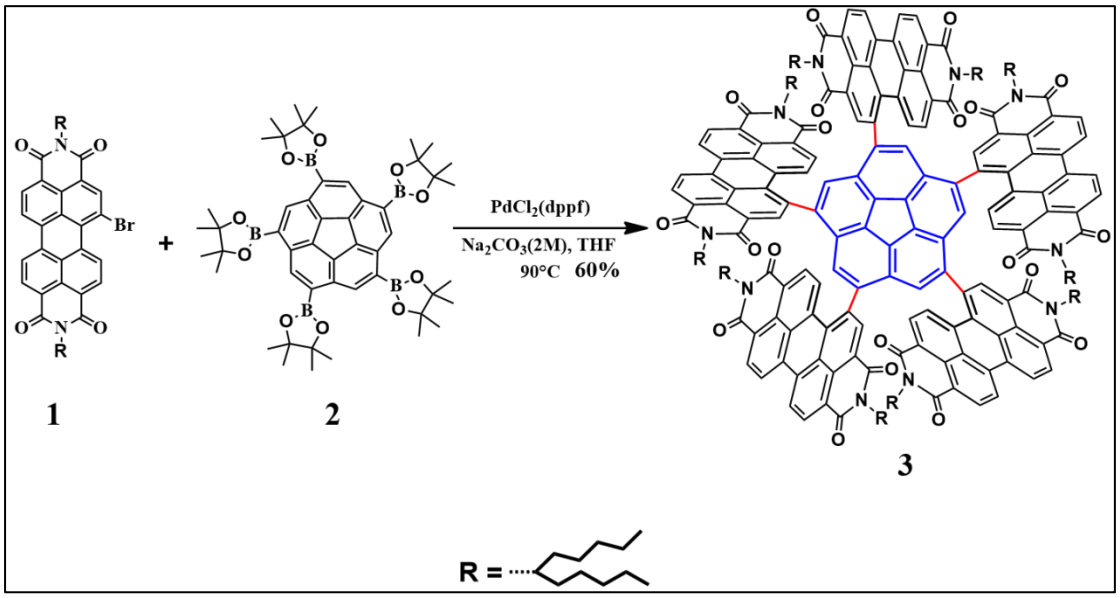

Compound 3: A Schlenk flask was charged with 1,3,5,7,9-pentakis(pinacolatoboryl)corannulene (**2:** 100 mg, 0.11 mmol ,1.0 equiv), 1-bromo-perylene-3,4,9,10-tetracarboxylic diimides (**1:** 486 mg, 0.62 mmol, 5.5 equiv), THF (6 ml) and Na_2CO_3 aqueous solution (2M, 3 ml). The mixture was degassed with argon for 15min. $PdCl_2$(dppf) (30 mg, 0.03 mmol, 0.3 equiv) was added under an argon atmosphere. The mixture was refluxed for 72 h and then cooled down to room temperature. The cooled mixture was poured into 1M HCl aqueous solution (500 ml) and stirred for 2 h. The precipitate was collected by vacuum filtration, washed with water and CH_3OH, dried, and purified by column chromatography on silica gel, eluted with petroleum ether/CH_2Cl_2 (1:1 to 1:5 v/v) to afford compound **3** (254 mg, 60% yield) as dark red solids.

^{1}H NMR (500 MHz, $C_2D_2Cl_4$, 298.5 K) δ = 8.81-8.39 (m, 26 H), 8.07-7.24 (m, 14 H), 5.23-4.71 (m, 10 H), 2.36-1.82 (m, 35 H), 1.37-1.18 (m, 105 H), 0.96-0.28 (m, 72 H); ^{13}C NMR (125 MHz, $C_2D_2Cl_4$, 298.5 K): δ =163.88, 163.38, 162.78, 162.14, 161.30, 144.71, 137.39, 136.47, 135.71, 134.55, 134.13, 133.47, 132.93, 131.70, 131.09, 130.56, 130.28, 130.01, 129.06, 128.87, 128.24, 126.84, 126.24, 124.44, 123.56, 122.62, 121.93, 54.79, 53.53, 52.42, 51.73, 33.71, 33.07, 32.58, 32.01, 31.52,

30.11, 26.47, 25.23, 24.65, 24.39, 23.03, 22.76, 22.50, 21.91, 21.50, 14.54, 14.33, 14.15, 13.84, 13.13, 12.83, 12.24; HRMS (MALDI(N), 100%): calcd (%) for $C_{250}H_{270}N_{10}O_{20}$: 3732.04234; found, 3732.04293.

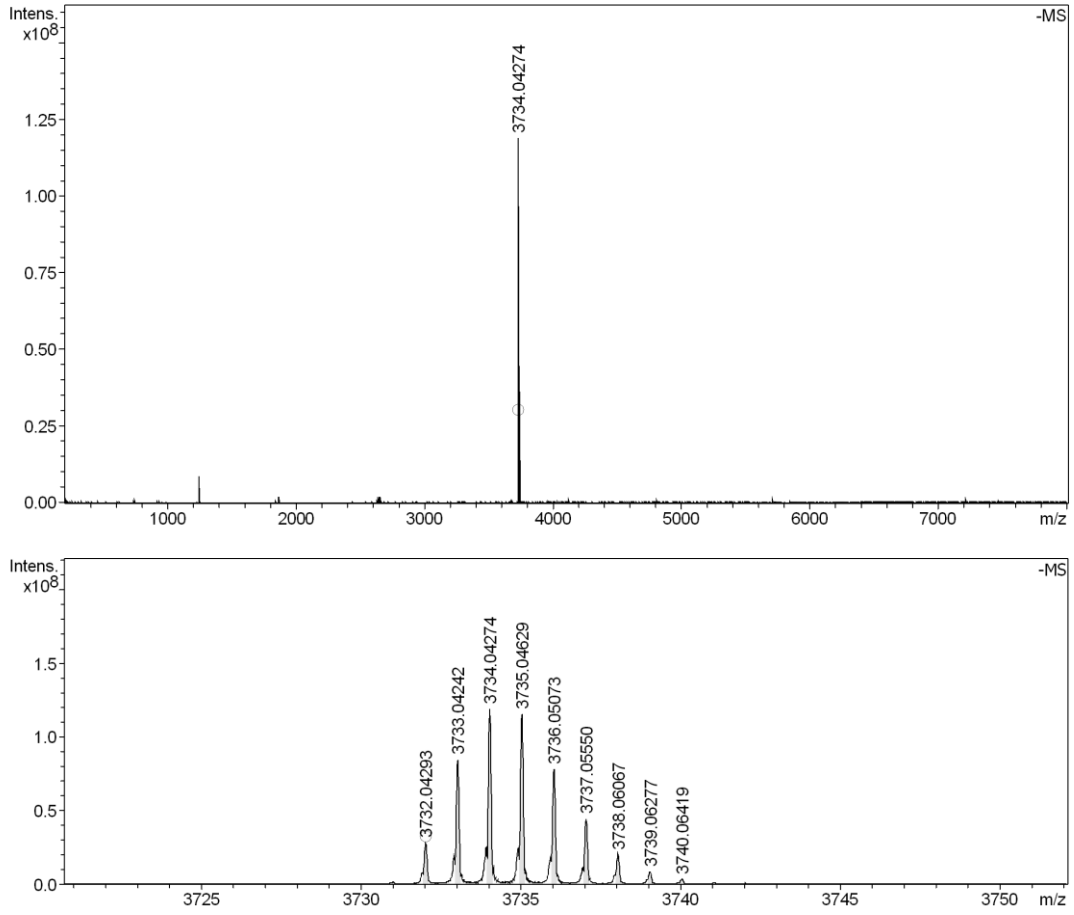

HR-MALDI-TOF mass spectrum of Compound **3**.

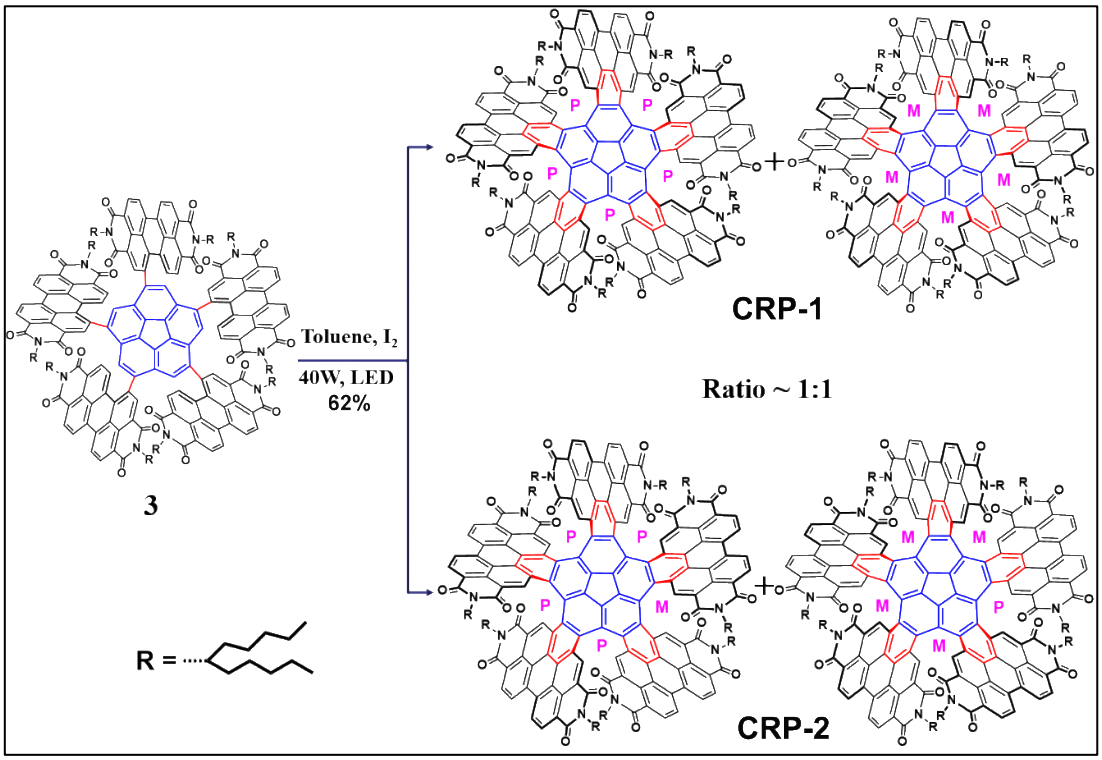

Compound CRP-1 and CRP-2: To a standard photocyclization glassware were added compound **3** (500 mg, 10 × 50 mg), toluene (500 ml, 10 × 50 ml) and I_2 (50 mg, 10 × 5 mg). The mixture was illuminated by 40 W mercury lamp for 72 h at 110 °C. The mixture was extracted with saturated sodium sulfite solution (2 × 500 ml) and concentrated under reduced pressure. The crude product was purified by column chromatography on silica gel, eluted with petroleum ether/CH_2Cl_2 (3:2 to 1:1 v/v) to afford **compound CRP-1** (first part) and **CRP-2** (second part) as red solids (Ratio ~ 1:1, 309 mg, 62% total yields).

Compound CRP-1: ^{1}H NMR (500 MHz, $C_2D_2Cl_4$, 373.2 K) δ = 9.59 (s, 10 H), 9.46-9.44 (d, *J* = 10 Hz, 10 H), 9.15-9.13 (d, *J* = 10 Hz, 10 H), 4.63 (s, 10 H), 1.64-1.57 (m, 25 H), 1.42 (s, 10 H), 1.25-1.20 (m, 85 H), 0.99-0.92 (m, 110 H); ^{13}C NMR (125 MHz, $C_2D_2Cl_4$, 373.2 K): δ = 162.70, 162.25, 133.79, 133.11, 132.11, 132.03, 129.04, 128.32, 126.04, 124.77, 123.57, 122.48, 122.27, 121.64, 120.90, 53.26, 30.94, 30.88, 30.58, 30.40, 25.34, 25.08, 21.36, 21.17, 12.88; HRMS (MALDI(N), 100%): calcd (%) for $C_{250}H_{260}N_{10}O_{20}$: 3721.96409; found, 3721.96240.

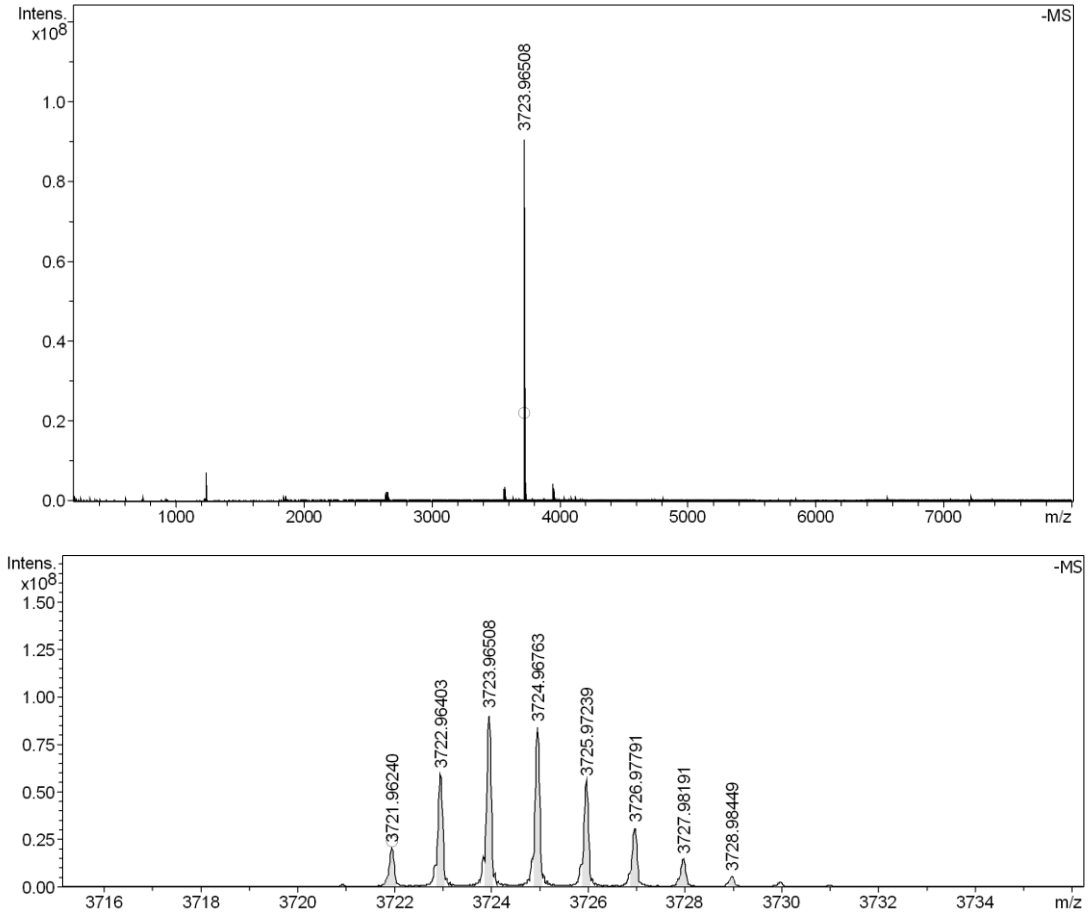

HR-MALDI-TOF mass spectrum of **CRP-1**.

Compound CRP-2: ^{1}H NMR (500 MHz, $C_2D_2Cl_4$, 373.2 K) δ = 10.59 (s, 2 H), 10.42 (s, 2 H), 9.74 (s, 2 H), 9.55-9.51 (q, J_1 = 5 Hz, J_2 = 10 Hz, J_3 = 5 Hz, 4 H), 9.48 (s, 2 H), 9.45-9.44 (d, J = 5 Hz, 3 H), 9.42-9.40 (m, 5 H), 9.26-9.25 (d, J = 5 Hz, 2 H), 9.17-9.11 (q, J_1 = 10 Hz, J_2 = 10 Hz, J_3 = 10 Hz, 6 H), 9.05-9.04 (d, J = 5 Hz, 2 H), 5.08 (s, 2 H), 4.83-4.66 (m, 8 H), 2.14-1.87 (m, 9 H), 1.65 (m, 22 H), 1.35-0.78 (m, 199 H); ^{13}C NMR (125 MHz, $C_2D_2Cl_4$, 373.2 K): δ = 163.79, 162.97, 136.01, 135.62, 135.17, 134.51, 134.22, 134.15, 133.99, 133.71, 133.10, 132.52, 131.05, 130.04, 129.10, 127.91, 127.55, 127.20, 127.07, 126.70, 126.02, 125.91, 125.71, 125.48, 125.31, 124.80, 124.53, 123.46, 122.68, 121.89, 54.50, 54.35, 32.25, 32.11, 31.98, 31.66, 31.60, 31.51, 31.42, 31.27, 29.61, 26.51, 26.43, 26.22, 22.37, 22.26, 22.13, 13.85; HRMS (MALDI(N), 100%): calcd (%) for $C_{250}H_{260}N_{10}O_{20}$: 3721.96409; found, 3721.96462.

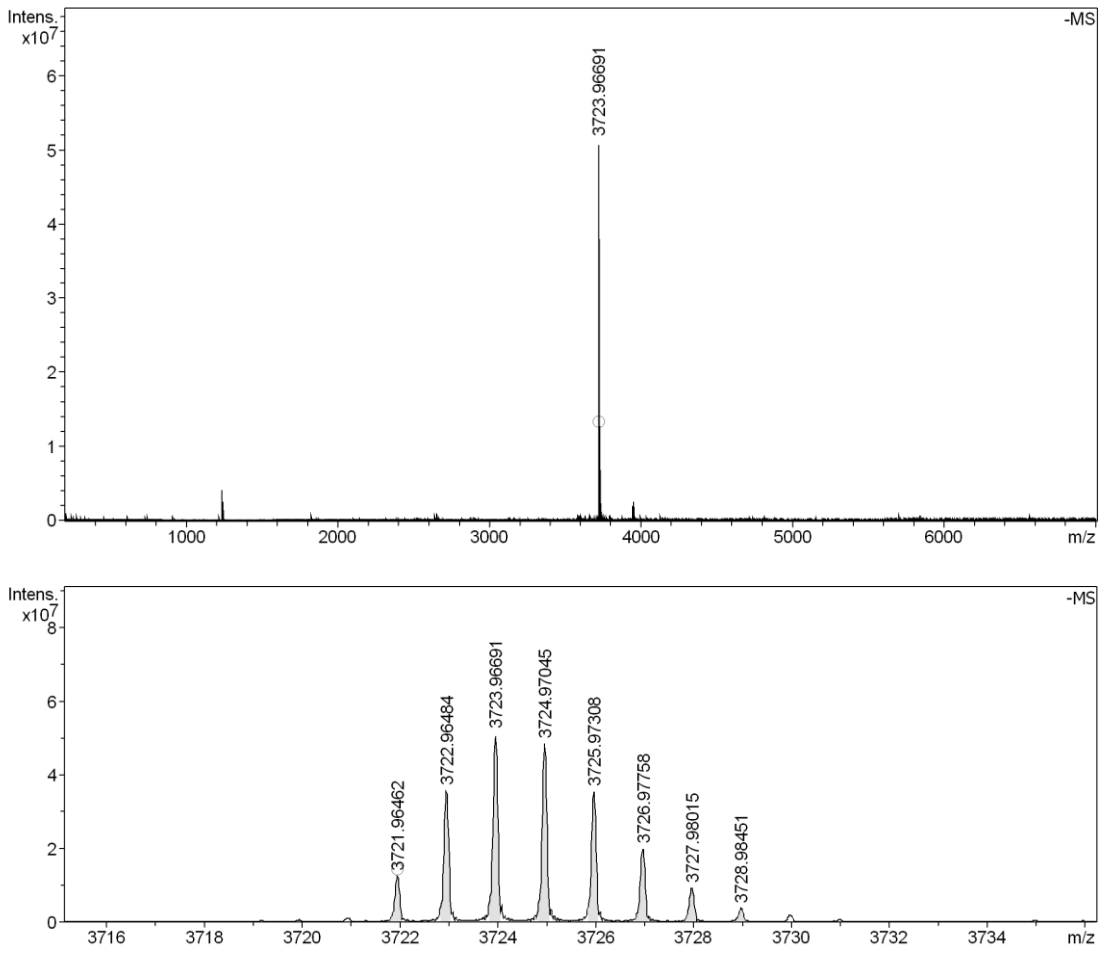

HR-MALDI-TOF mass spectrum of **CRP-2**.

Computational Methods Details:

I. The structural and energetic analyses of the molecular systems described in this study were investigated with two types of density functional methods, B3LYP-D3[2,3] and wB97-D[4], and several basis set types, specifically shown here are 6-311G(2d,p)[5-7] and Def2-TZVP[8] basis sets. All provided consistent results; B3LYP-D3/6-311G(2d,p) and B3LYP-D3/Def2-TZVP are shown here, and the former used in the discussion in the paper. All calculations employed an ultrafine grid. Full geometry optimizations were performed and uniquely characterized via second derivatives (Hessian) analysis to establish stationary points and effects of zero point energy. Visualization and analysis of structural and property results were obtained using Avogadro.[9]

Table S1. The energetic analyses of four isomers.

Molecule	B3LYP-D3/6-311G(2d,p) (kcal/mol)		B3LYP-D3/Def2-TZVP (kcal/mol)	
	ΔH	**ΔG**	**ΔH**	**ΔG**
CRP-1	0.0	0.0	0.0	0.0
CRP-2	5.00	5.53	5.7	6.2
CRP-3	5.56	6.03	6.3	6.8
CRP-4	9.95	11.4	11.2	12.6

Orbital structure for optimized CRP-1, D_5 symmetry

	HOMO-3	HOMO-2	HOMO-1	HOMO
	592	593	594	595
	(E1)--O	(E1)--O	(E2)--O	(E2)--O
Eigenvalues --	-0.23555	-0.23555	-0.22300	-0.22300

	LUMO	LUMO+1
	596	597
	(E2)--V	(E2)--V
Eigenvalues --	-0.13721	-0.13721

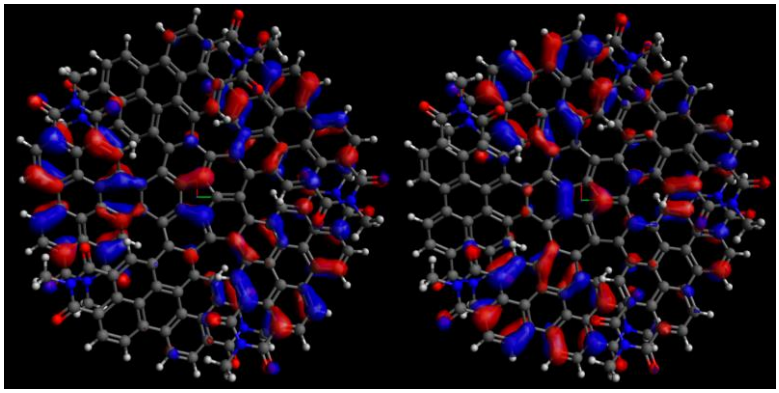

HOMO-3 **HOMO-2**

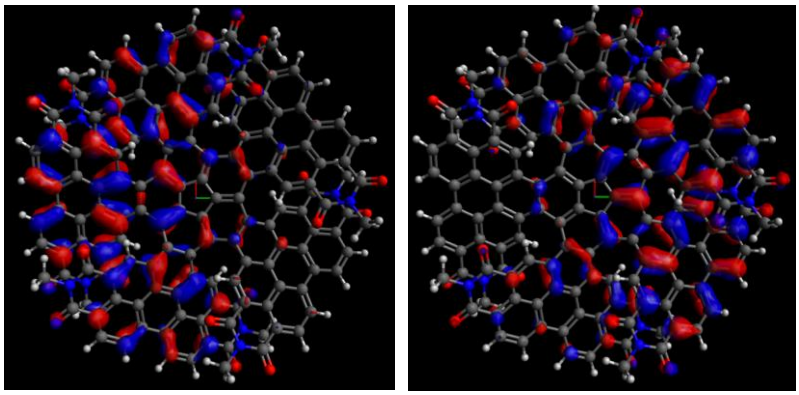

HOMO-1 **HOMO**

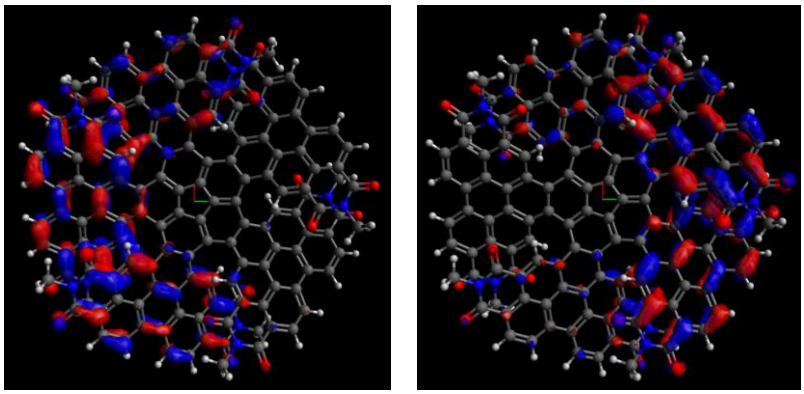

LUMO **LUMO+1**

II. Nucleus-independent chemical shifts (NICS) properties,[10] including NICS(Iso),[11,12] NICS(In-plane), and NICS(ZZ)[13] values, were investigated using the GIAO method[14,15] and compared at B3LYP-D3/6-311+G(2d,p),[5-7] B3LYP-D3/6-311+G(2df,pd),[5-7] and B3LYP-D3/Def2-TZVP levels of theory, all of which provided consistent results. The isotropic chemical shift values are separated into their in-plane (NICS(Iso)) and out-of-plane (NICS(ZZ)) components, by consideration of the eigenvalues of the chemical shift tensors. The NICS(ZZ) values, more closely related to the current density, reflect the magnetic response of a molecule toward a magnetic field applied perpendicular to the plane (i.e., z direction), and are therefore considered primarily associated with the π contribution. Graphical visualization of the results were carried out with the KaleidaGraph software.

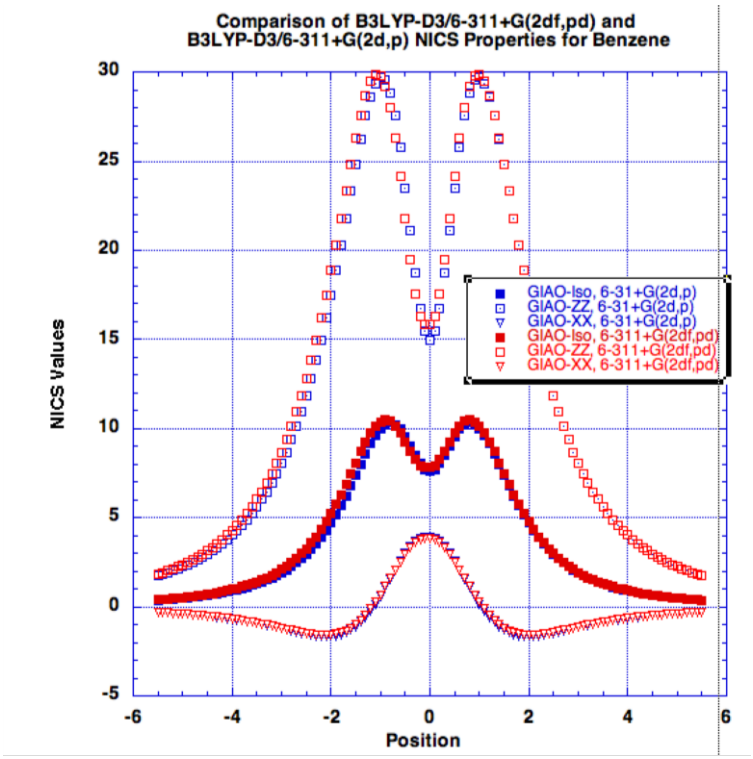

Figure S1. B3LYP/6-311+G(2d,p) (blue) and B3LYP/6-311+G(2df,pd) (red) calculated NICS values along the symmetry axis for benzene D_{6h} symmetry.

III. Absorption energies were computed at the TD-B97xD[16]/6-311G(2d,p), TD-B97xD[16]/Def2-TZVP and TD-camB3LYP[17]/6-311G(2d,p), TD-camB3LYP[17]/Def2-TZVP levels of theory in gas phase and in chloroform, with consistent results. Representative spectra shown here carried out in chloroform.

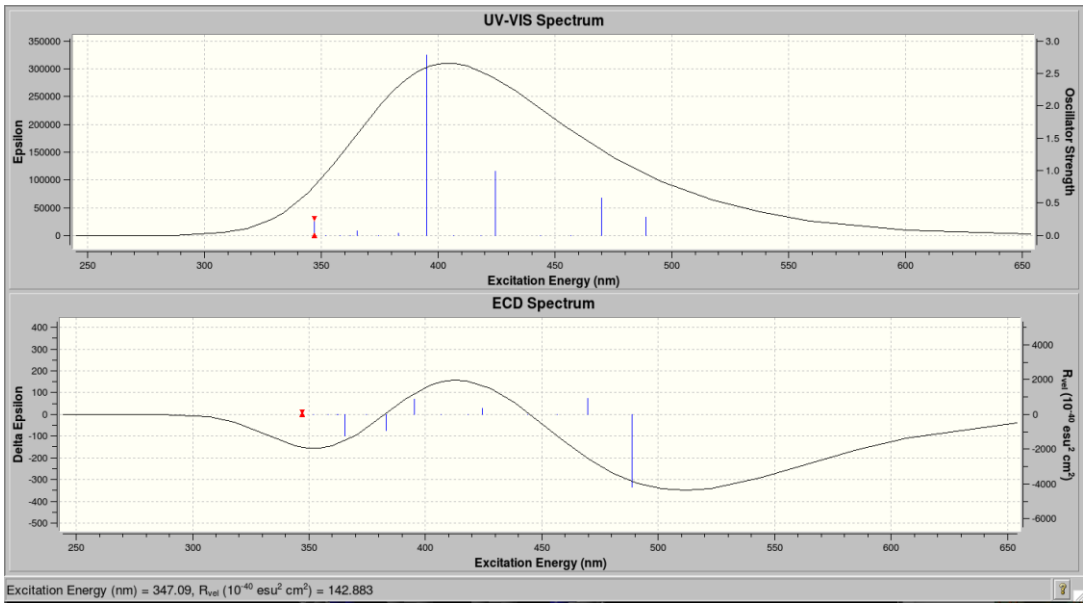

Figure S2. TD-B97xD/6-311G(2d,p) (chloroform) UV-Vis and ECD spectra for CRP-1.

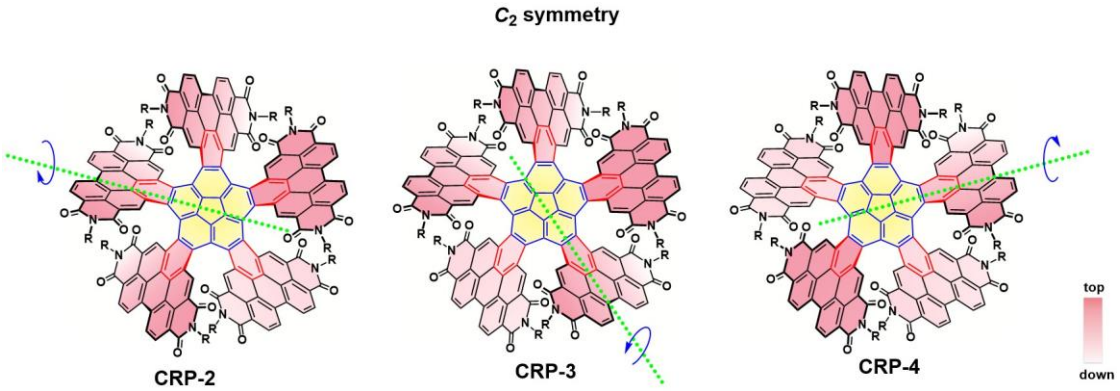

Figure S3. C_2 axis position of **CRP-2**, **CRP-3** and **CRP-4**.

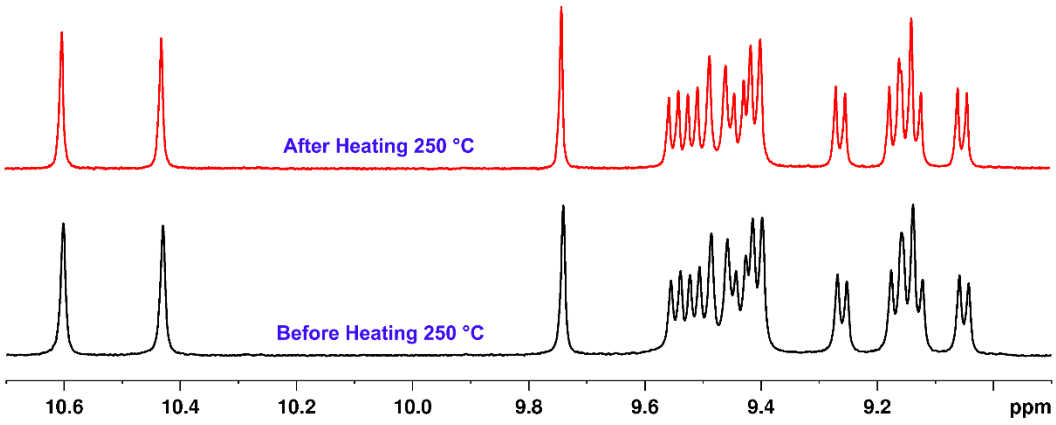

Figure S4. The ^{1}H NMR spectra of **CRP-2** before and after heating in the diphenyl ether at 250 °C for 6 hours. (500 MHz, $C_2D_2Cl_4$, 373.2 K)

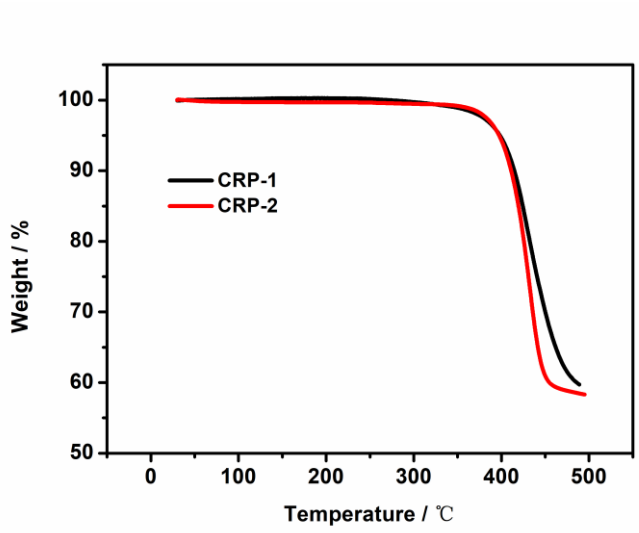

Figure S5. TGA curves of **CRP-1** and **CRP-2** under nitrogen flow.

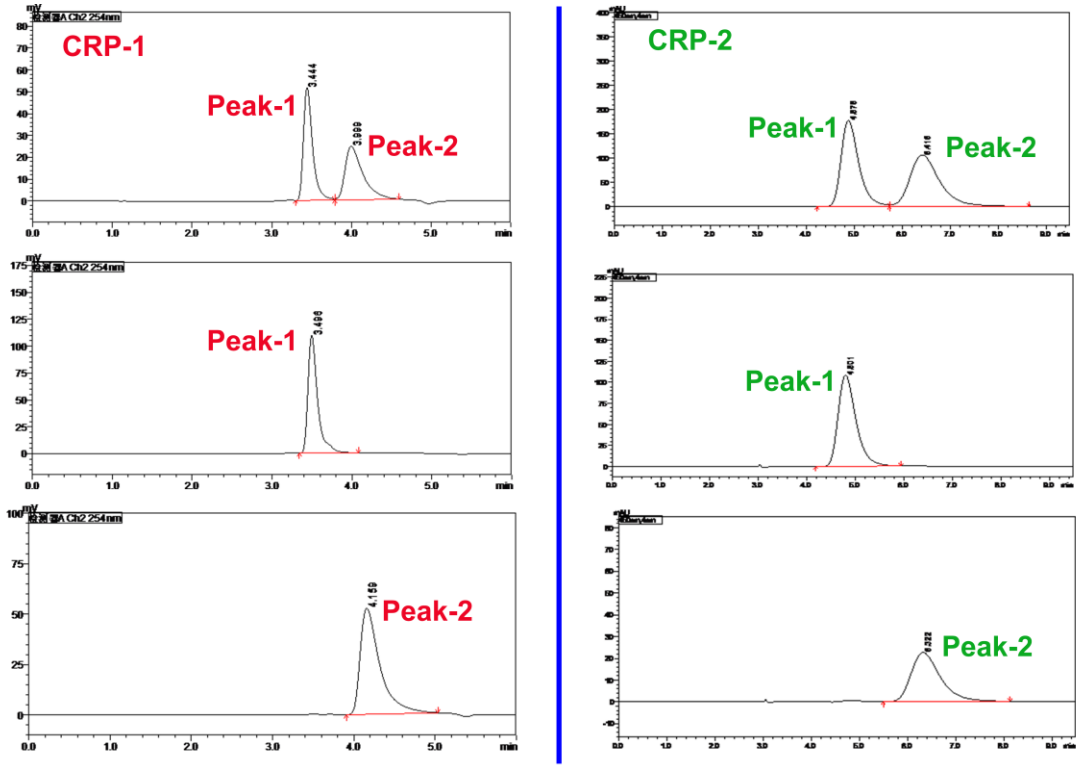

Figure S6. Chiral HPLC chromatogram of **CRP-1** (red) and **CRP-2** (green). The separation conditions: for **CRP-1**, CHIRALPAK AS-H (ASH0CE-PG009) column with *n*-hexane/Isopropyl alcohol/ Diethanolamine (99.8/0.2/0.05(V/V/V)) as eluent; for **CRP-2**, CHIRALPAK IG column with Hexane/EtOH (90/10(V/V)) as eluent.

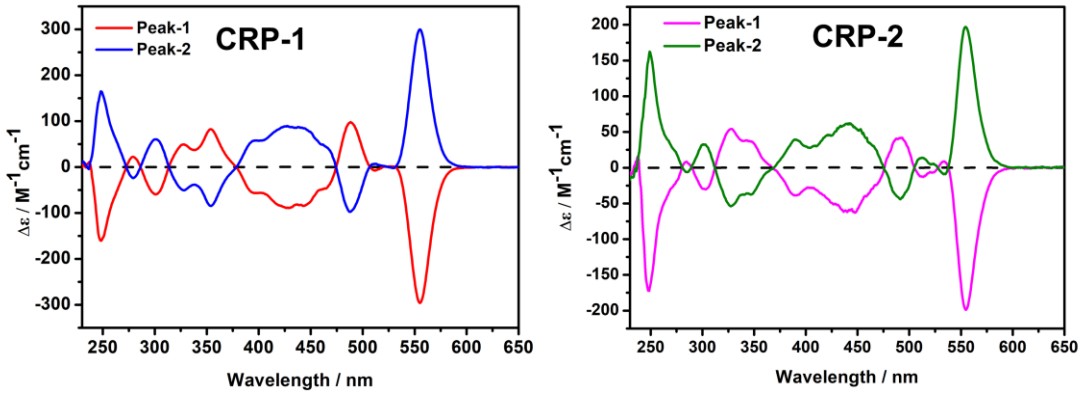

Figure S7. The CD spectra of **CRP-1** and **CRP-2** in $CHCl_3$ solution (1.0×10^{-5} M).

X-ray Crystal Structure

The single crystals were obtained by slow vapor diffusion method under the THF (good solvent) and CH_3OH (poor solvent). Single crystal data collections were performed at about 100 K and 170 K for **CRP-2** and **CRP-1** on a MD2 diffractometer and MM007HF Saturn724+ diffractometer, using adjustable graphite-monochromated radiation (λ=0.88557 Å) and Mo Kα radiation (0.71073 Å), respectively. Using Olex2, these structures were solved with the ShelXS and refined with the ShelXL-2014 refinement package using Least Squares minimization. Refinement was performed on F^2 anisotropically for all the non-hydrogen atoms by the full-matrix least-squares method. The hydrogen atoms were placed at the calculated positions and were included in the structure calculation without further refinement of the parameters. Because of the very large thermal motion and disorder of side chains in the lattice, the diffuse residual electron density is difficult to be accurately modeled and thus a treatment by SQUEEZE (from PLATON) was used to dissolve the disorder in the side chains. Despite many attempts, the diffraction intensity of **CRP-1** and **CRP-2** is very weak, which lead to their high R values and alerts of level A in checkCIF reports. Fortunately, the diffraction from the conjugated backbone could be easily confirmed, and we did not find any errors from the conjugated backbone.

Table S2. Crystallographic data and structure refinement details for **CRP-1** and **CRP-2**

	CRP-1	**CRP-2**
T (K)	173 (2)	100
λ (Å)	0.71073	0.88557
cryst syst	Trigonal	Triclinic
space group	*P*3c1	*P*-1
a, (Å)	31.791(5)	21.504(4)
b, (Å)	31.791(5)	22.883(5)
c, (Å)	45.798(9)	44.815(9)
α, (deg)	90.00	96.640(4)
β, (deg)	90.00	100.370(6)

γ, (deg)	120.00	109.800(9)
V, (Å^3)	40085(11)	20035(7)
Z	6	2
D_{calc}, (g / cm^3)	0.731	0.960
μ (mm^{-1})	0.047	0.063
F(000)	9252	6072
Theta range, (deg)	0.74-25.01	0.94-20.99
reflns collected	345743	256413
indep reflns/R_{int}	47156 / 0.1201	39076 / 0.1962
params	2035	4002
GOF on F^2	1.519	1.973
R_1, wR_2 [I>2σ(I)]	0.2756 / 0.5701	0.2807 / 0.5710
R_1, wR_2 (all data)	0.3206 / 0.6104	0.3473 / 0.6103

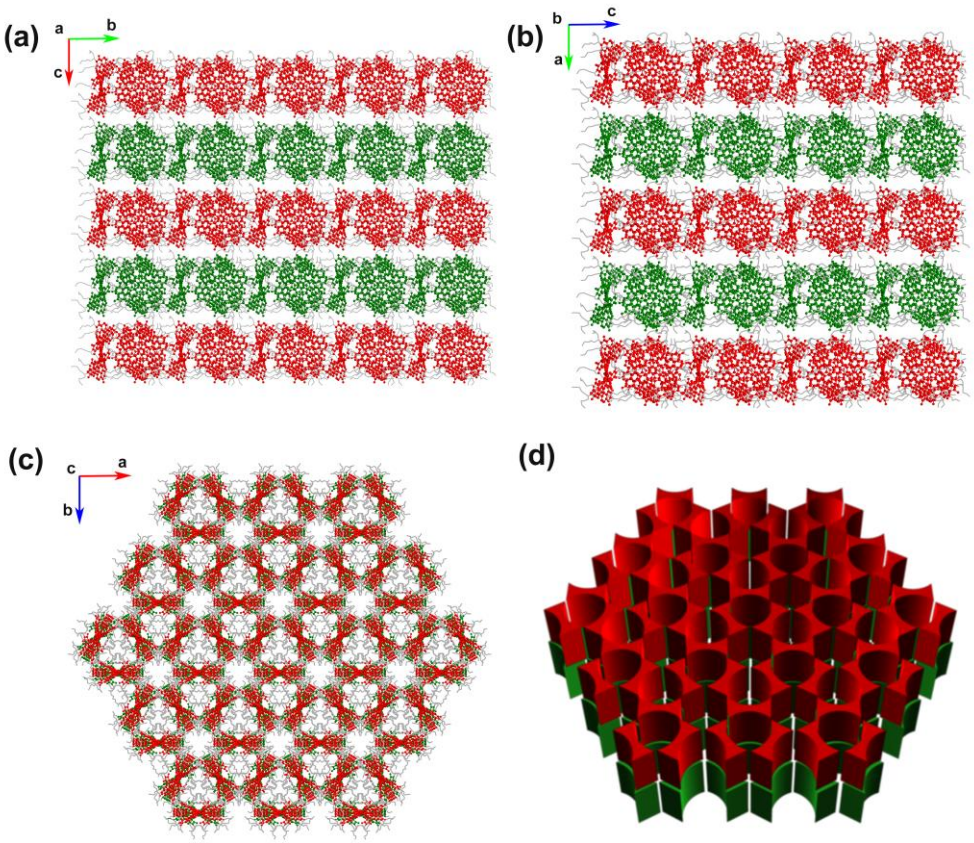

Figure S8. The crystal 3D-stacking model of **CRP-1** with side chains (a) (b) (c) and schematic diagram (d) (along the *c* axis).

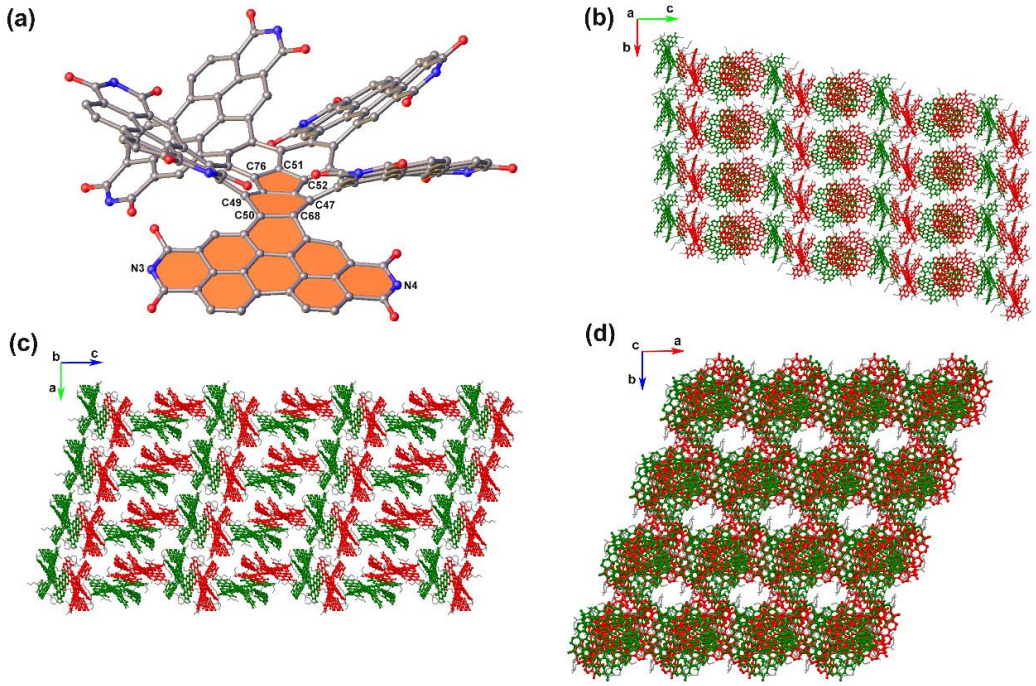

Figure S9. (a) The relatively planar component of **CRP-2** consisting of down PDI petal and part of the corannulene core (orange part) and (b) (c) (d) the crystal 3D-stacking model of **CRP-2** with part of side chains.

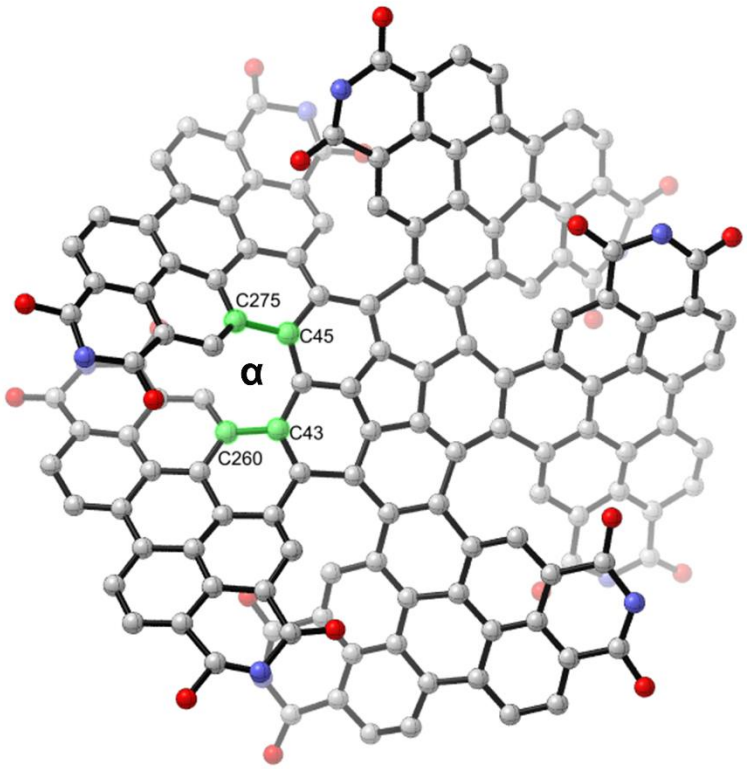

Figure S10. The definition of torsion angle α.

Transistor Device Fabrication and Characterization: The substrates used here were successively cleaned with pure water, piranha solution (H_2SO_4/H_2O_2 = 7:3), pure water, pure isopropyl alcohol, and finally blown dry with high-purity nitrogen gas. Treatment of the Si/SiO_2 wafers with OTS was carried out by the vapor-deposition method. The clean wafers were dried under vacuum at 90 ℃ for 0.5 h in order to eliminate the influence of moisture. When the temperature decreased to 70 °C, a small drop of OTS was placed around the wafers. Subsequently, this system was heated to 120 ℃ and maintained for 2 h under vacuum.

Micro-/nano-crystals were fabricated by the use of a dilute $CHCl_3$ solution (1 mg mL^{-1}). Bottom-gate top-contact OFETs based on the micro-/nano-crystals were constructed on an OTS modified Si/SiO_2 substrate (n-type Si wafer containing 300 nm-thick SiO_2) using an "organic ribbon mask" technique. Prior to the self-assembly of micro-/nano-crystals, the OTS modified Si/SiO_2 substrate was cleaned with pure n-hexane, pure chloroform, and pure isopropyl alcohol. Then, micro-/nano-crystals were produced on Si/SiO_2 substrates through drop casting. Subsequently, 40 nm thick source and drain electrodes were deposited on the micro-/nano-crystals by thermal evaporation. Electrical characteristics of the devices were tested with a Keithley 4200-SCS semiconductor parameter analyzer and a Micromanipulator 6150 probe station in a glove box at room temperature. The mobilities were calculated from the saturation region with the following equation: $I_{DS} = (W/2L)\, C_i \mu\, (V_G - V_T)^2$, where I_{DS} is the drain–source current, W is the channel width, L is the channel length, μ is the field-effect mobility, C_i is the capacitance per unit area of the gate dielectric layer, and V_G and V_T are the gate voltage and threshold voltage, respectively. This equation defines the important characteristics of electron mobility (μ), on/off ratio ($I_{on/off}$), and threshold voltage (V_T), which could be deduced by the equation from the plot of current–voltage.

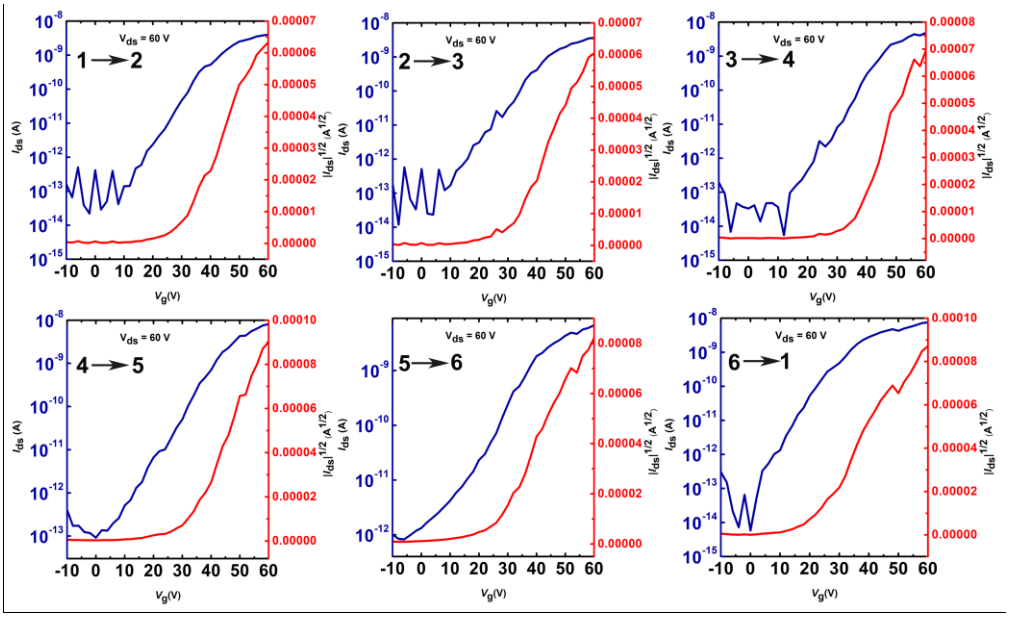

Figure S11 Transfer curves of six OFET devices with different crystal planes.

Table S3. Field-effect electron (e) mobility of six OFET devices with different crystal planes.

Channels	1 ⟷ 2	2 ⟷ 3	3 ⟷ 4	4 ⟷ 5	5 ⟷ 6	6 ⟷ 1
μ [$cm^2/(V•s)$]	5.92×10^{-4}	5.69×10^{-4}	7.32×10^{-4}	6.69×10^{-4}	9.64×10^{-4}	6.92×10^{-4}
I_{on}/I_{off}	1.82×10^{5}	3.08×10^{5}	8.84×10^{5}	8.84×10^{4}	8.17×10^{3}	1.30×10^{6}

Table S4. The mobilities in thin-film devices made of CRP-1 and CRP-2 by spin-coating method (Solvent: $CHCl_3$; 3000 rpm; Concentration: 10 mg/ml).

Devices	W/L (μm)	$Mobility^{ave}$ ($cm^2\ V^{-1}\ s^{-1}$)	$Mobility^{max}$ ($cm^2\ V^{-1}\ s^{-1}$)	V_T (V)	On/off Ratio
CRP-1	1400/10	9.22×10^{-4}	1.32×10^{-3}	-5.1	3.2×10^{6}
CRP-2		7.03×10^{-4}	8.19×10^{-4}	-5.4	4.9×10^{5}

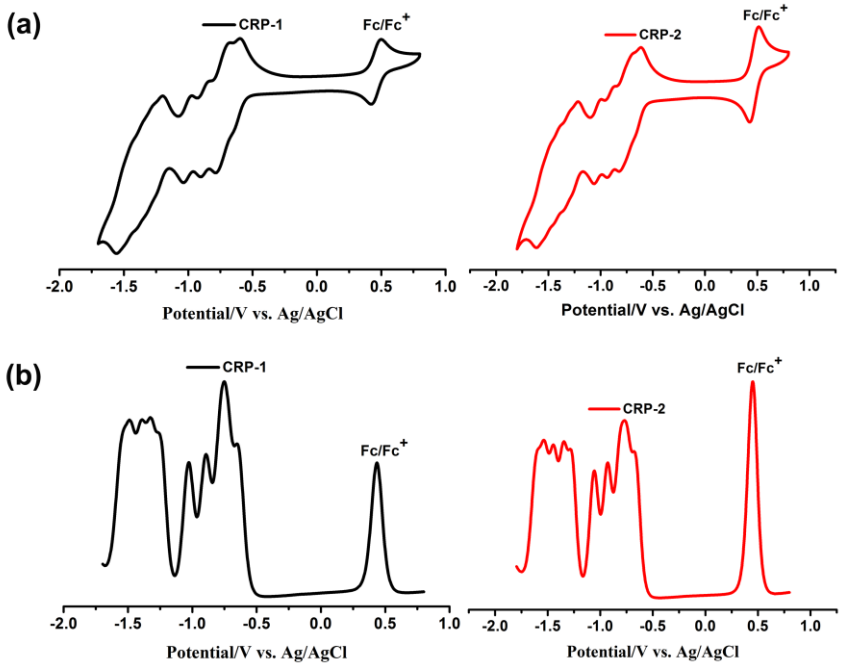

Figure S12. Cyclic voltammetries (a) and DPV profiles (b) of **CRP-1** and **CRP-2** in CH_2Cl_2.

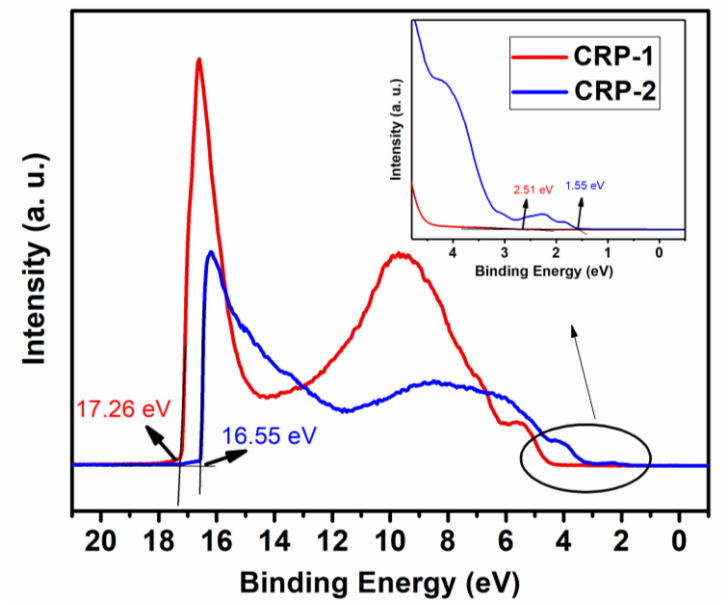

Figure S13. UPS characterization of **CRP-1** and **CRP-2** solids

The work function (WF) and ionization potential (IP) of CRP-1 and CRP-2 samples were measured by ultraviolet photoemission spectroscopy (UPS). As shown in Figure S13, the binding energy cutoff (E_{cutoff}) values of CRP-1 and CRP-2 samples are 17.26 and 16.55 eV, respectively. Accordingly, the calculated WF and IP of CRP-1 samples are 3.96 eV and 6.47 eV, CRP-2 samples are 4.67 eV and 6.22 eV, respectively.

^{1}H NMR and ^{13}C NMR Spectra of Products

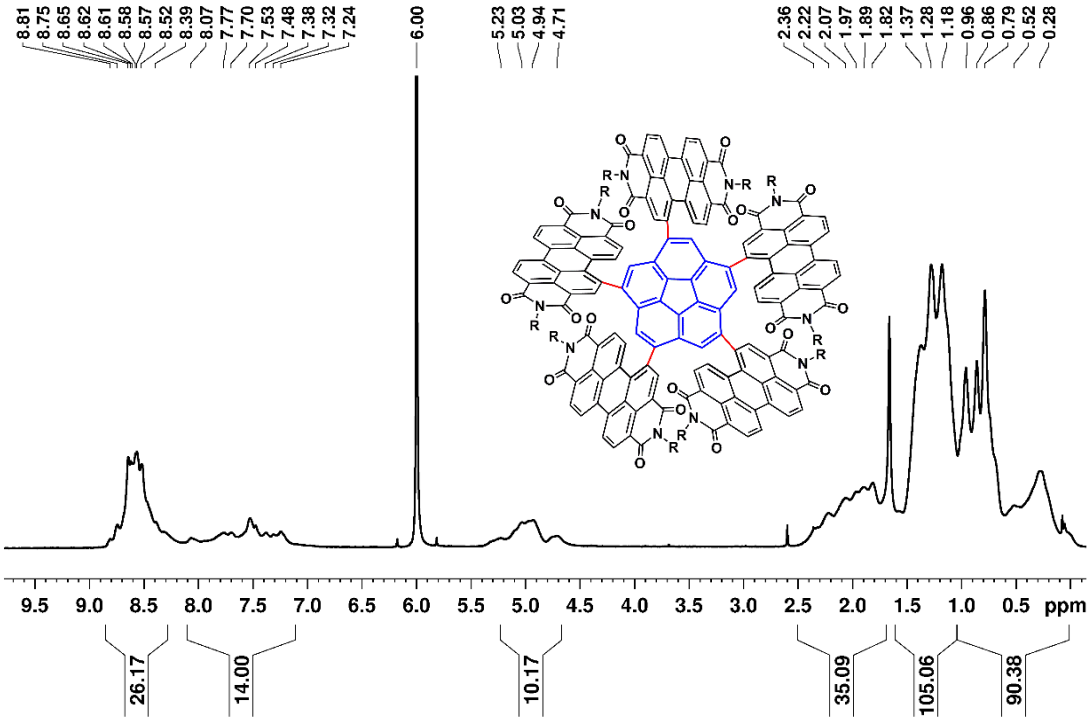

^{1}H NMR Spectra of Compound **3** (500 MHz, $C_2D_2Cl_4$, 298.5 K)

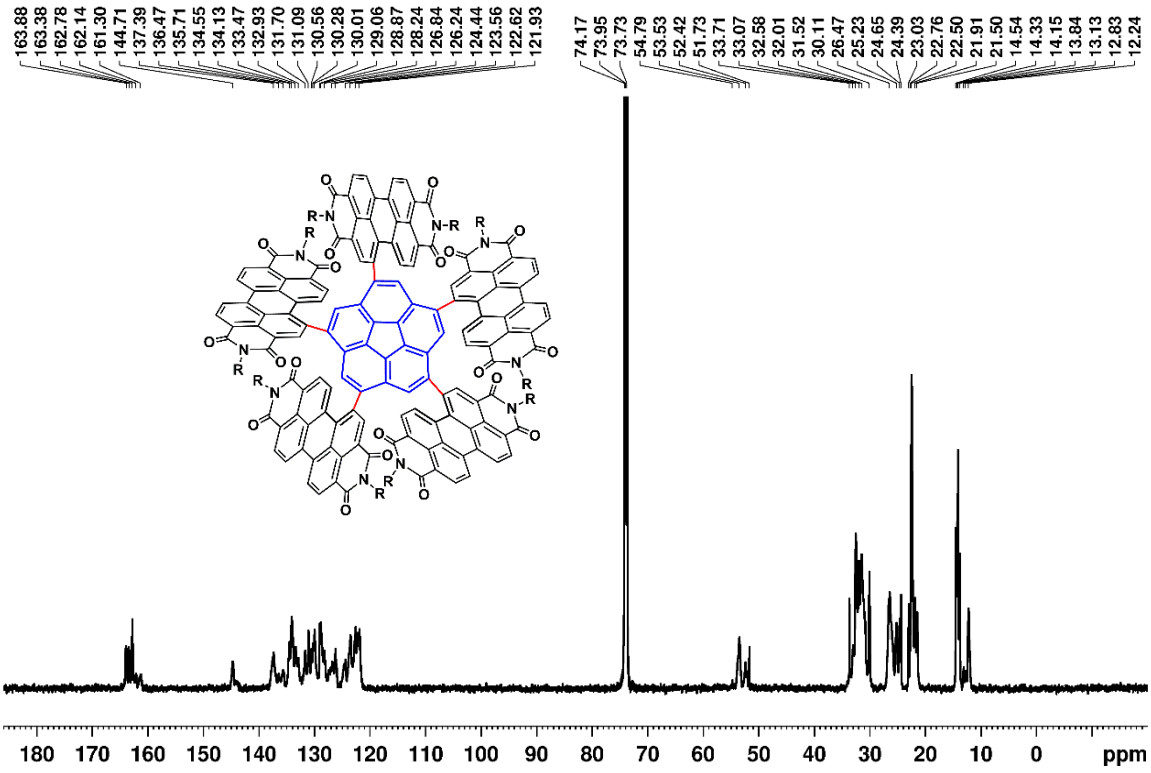

^{13}C NMR Spectra of Compound **3** (500 MHz, $C_2D_2Cl_4$, 298.5 K)

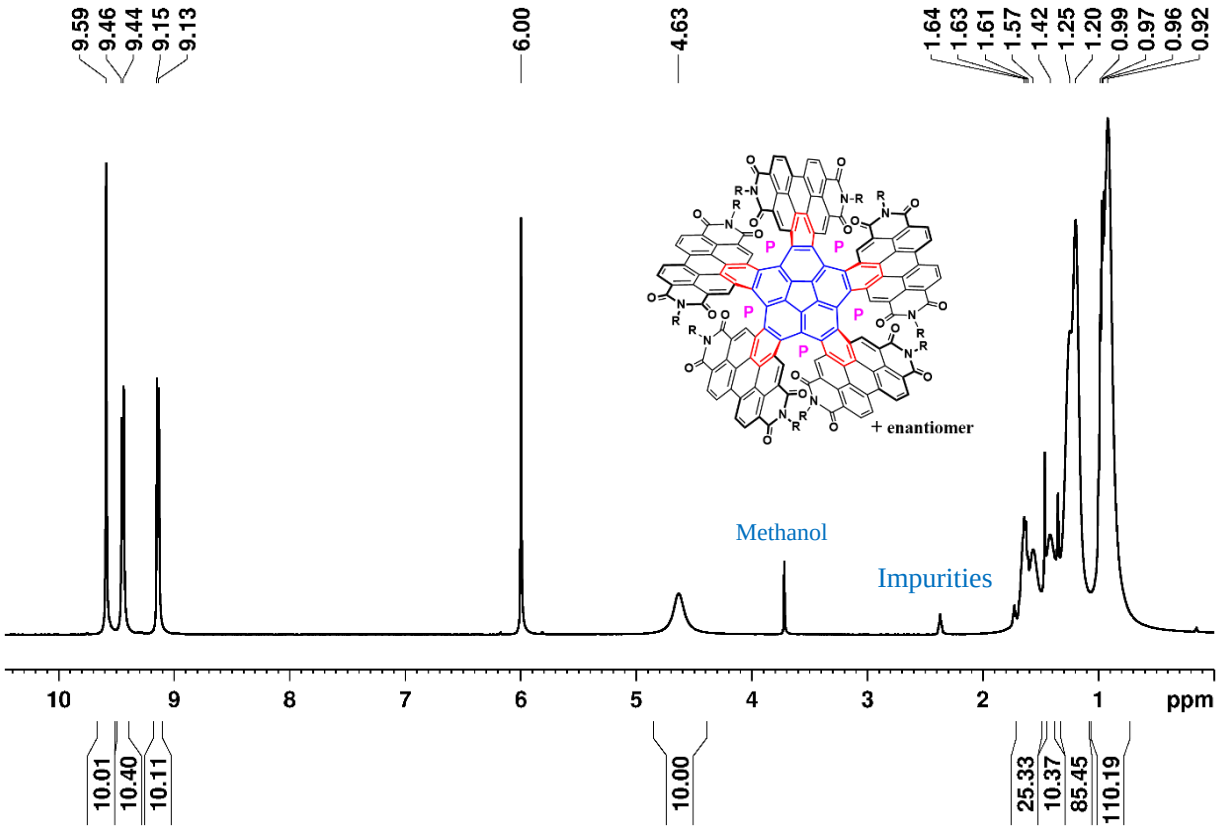

^{1}H NMR Spectra of **CRP-1** (500 MHz, $C_2D_2Cl_4$, 373.2 K)

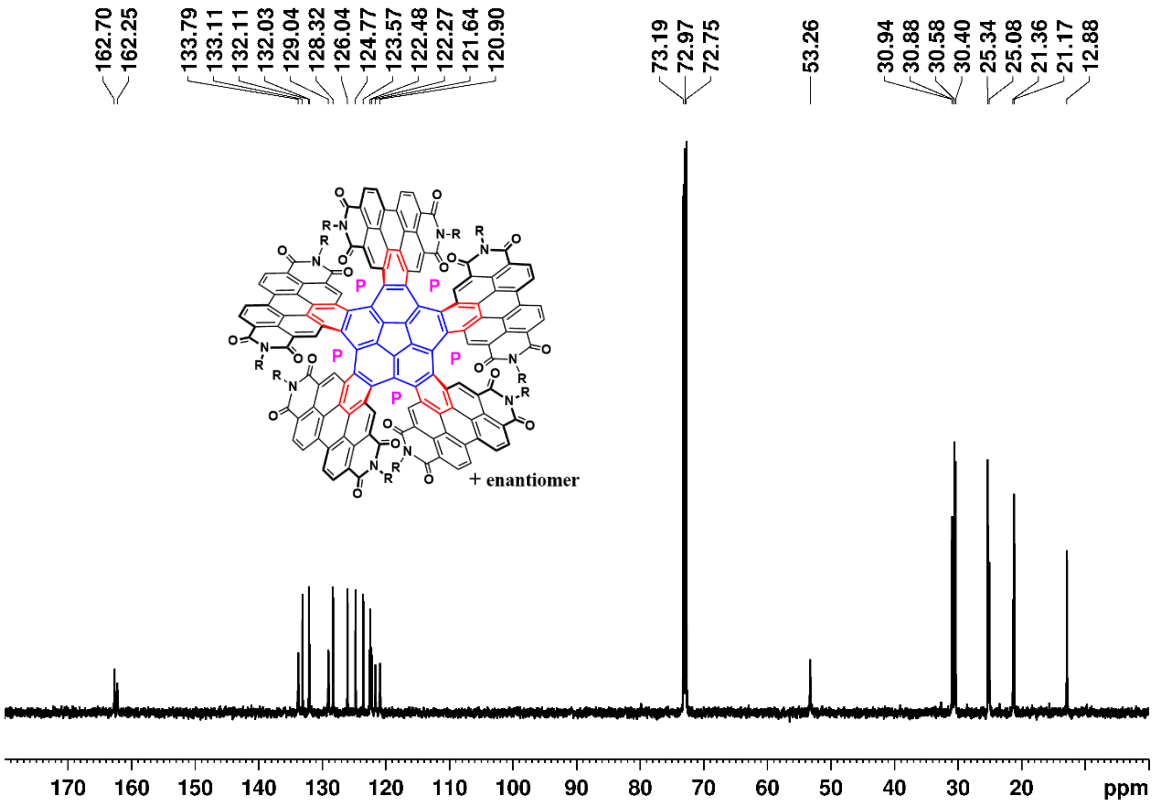

^{13}C NMR Spectra of **CRP-1** (500 MHz, $C_2D_2Cl_4$, 373.2 K)

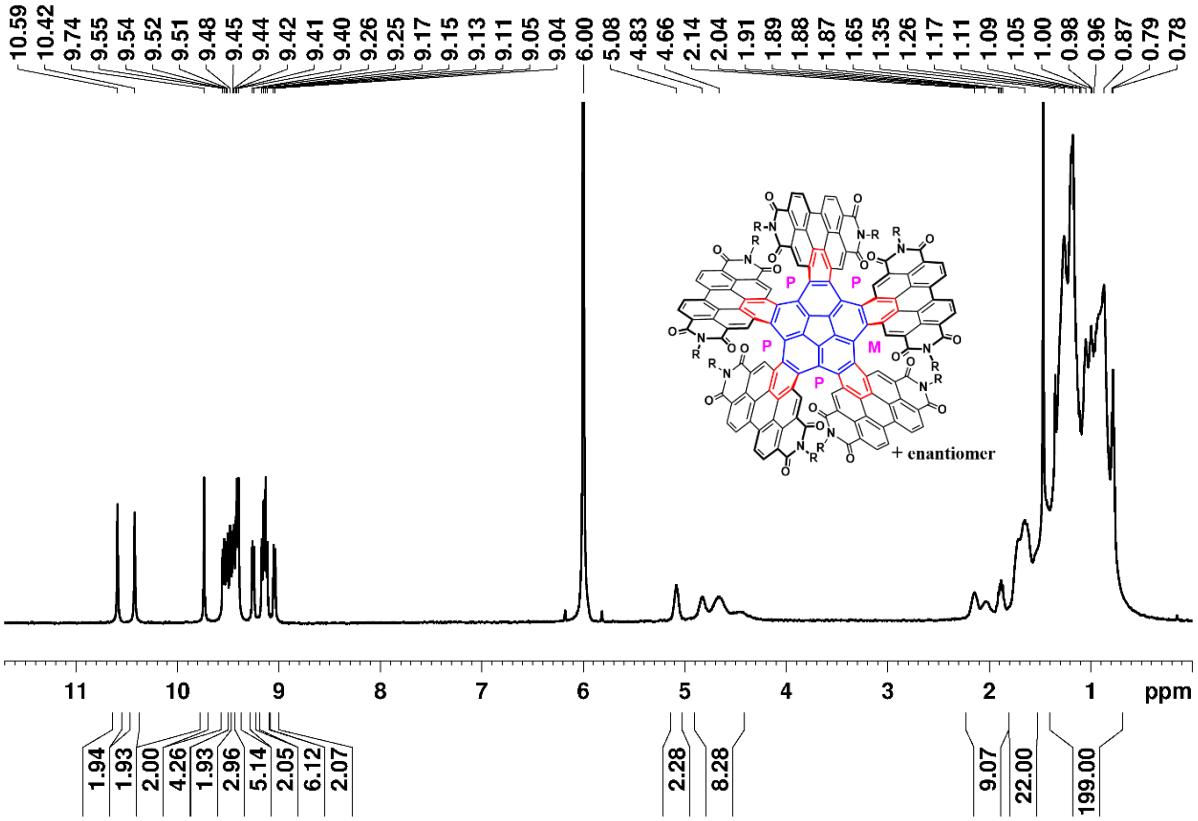

^{1}H NMR Spectra of **CRP-2** (500 MHz, $C_2D_2Cl_4$, 373.2 K)

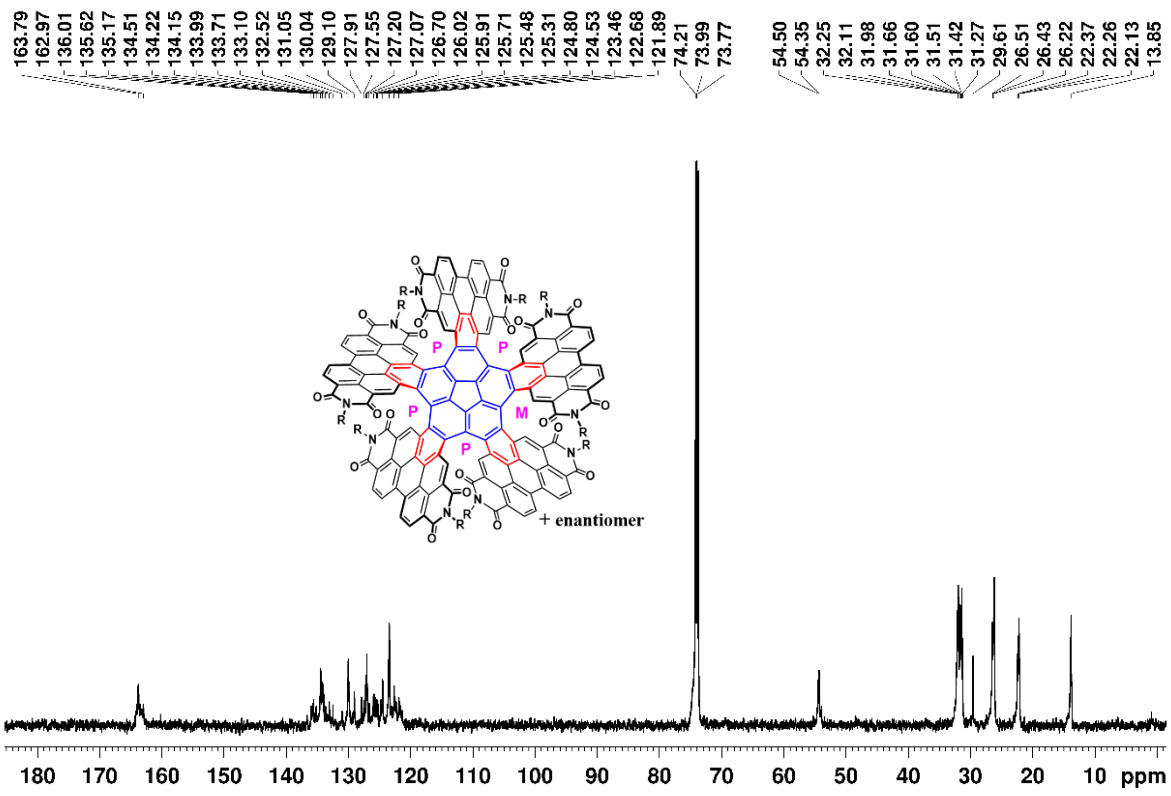

^{13}C NMR Spectra of **CRP-2** (500 MHz, $C_2D_2Cl_4$, 373.2 K)

References

(1) (a) Sun, D.; Meng, D.; Cai, Y.; Fan, B.; Li, Y.; Jiang, W.; Huo, L.; Sun, Y.; Wang, Z. Non-Fullerene-Acceptor-Based Bulk-Heterojunction Organic Solar Cells with Efficiency over 7%. *J. Am. Chem. Soc.* **2015**, *137*, 11156-11162. (b) Meng, D.; Sun, D.; Zhong, C.; Liu, T.; Fan, B.; Huo, L.; Li, Y.; Jiang, W.; Choi, H.; Kim, T.; Kim, J. Y.; Sun, Y.; Wang, Z.; Heeger, A. J. High-Performance Solution-Processed Non-Fullerene Organic Solar Cells Based on Selenophene-Containing Perylene Bisimide Acceptor. *J. Am. Chem. Soc.* **2016**, *138*, 375-380.

(2) Becke, A. D., Density-Functional Thermochemistry. III. The Role of Exact Exchange. *J. Chem. Phys.* **1993,** *98*, 5648-5652.

(3) Grimme, S.; Antony, J.; Ehrlich, S.; Krieg, H. A Consistent and Accurate ab Initio Parametrization of Density Functional Dispersion Correction (DFT-D) for the 94 Elements H-Pu. *J. Chem. Phys.* **2010,** *132*, 154104.

(4) Chai, J.-D.; and Head-Gordon, M. Systematic Optimization of Long-Range Corrected Hybrid Density Functionals. *J. Chem. Phys.* **2008**, *128*, 084106.

(5) Ditchfield, R.; Hehre, W. J.; and Pople, J. A. Self-Consistent Molecular-Orbital Methods. IX. An Extended Gaussian-Type Basis for Molecular-Orbital Studies of Organic Molecules. *J. Chem. Phys.* **1971**, *54*, 724-728.

(6) McLean, A. D.; Chandler, G. S. Contracted Gaussian Basis Sets for Molecular Calculations. 1.Second Row Atoms, Z = 11−18. *J. Chem. Phys*. **1980,** *72***,** 5639−5648.

(7) Krishnan, R.; Binkley, J. S.; Seeger, R.; Pople, J. A. Self-Consistent Molecular Orbital Methods. XX. Basis Set for Correlated Wave Functions. *J. Chem. Phys*. **1980,** *72***,** 650−654.

(8) Weigend, F.; Ahlrichs, R. Balanced Basis Sets of Split Valence, Triple Zeta Valence and Quadruple Zeta Valence Quality for H to Rn: Design and Assessment of Accuracy. *Phys. Chem. Chem. Phys.*, **2005**, *7*, 3297-3305.

(9) Hanwell, M. D.; Curtis, D.; Lonie, D. C.; Vandermeersch, T.; Zurek, E.; Hutchison, G. R. Avogadro: An Advanced Semantic Chemical Editor, Visualization, and Analysis Platform. *J. Cheminform*. **2012**, *4*, 17.

(10) Schleyer, P. V. R.; Maerker, C.; Dransfeld, A.; Jiao, H.; Hommes, N. Nucleus-Independent Chemical Shifts: A Simple and Efficient Aromaticity Probe. *J. Am. Chem. Soc.* **1996**, *118*, 6317-6318.

(11) Schleyer, P. V. R.; Jiao, H.; Hommes, N.; Malkin, V. G.; Malkina, O. L. An Evaluation of the Aromaticity of Inorganic Rings: Refined Evidence from Magnetic Properties. *J. Am. Chem. Soc*. **1997**, *119*, 12669-12670.

(12) Schleyer, P. V. R.; Manoharan, M.; Wang, Z.-X.; Kiran, B.; Jiao, H.; Puchta, R.; Hommes, N. Dissected Nucleus-Independent Chemical Shift Analysis of π-Aromaticity and Antiaromaticity. *Org. Lett.* **2001**, *3*, 2465-2468.

(13) Cernusak, I.; Fowler, P. W.; Steiner, E. Ring Currents in Six-Membered Heterrocycles: the Diazaborinines $(CH)_2B_2N_2$. *Molec. Phys.* **2000**, *98*, 945-954.

(14) Wolinski, K.; Hinton, J. F.; Pulay, P. Efficient Implementation of the Gauge-Independent Atomic Orbital Method for NMR Chemical Shift Calculations. *J. Am. Chem. Soc*. **1990**, *112*, 8251-8260.

(15) Ditchfield, R. Molecular Orbital Theory of Magnetic Shielding and Magnetic Susceptibility. *J. Chem. Phys.* **1972**, *56*, 5688-5691.

(16) Chai, J.-D.; Head-Gordon, M. Long-Range Corrected Hybrid Density Functionals with Damped Atom-Atom Dispersion Corrections. *Phys. Chem. Chem. Phys.* **2008**, *10*, 6615-6620.

(17) Yanai, T.; Tew, D. P.; Handy, N. C. A New Hybrid Exchange-Correlation Functional Using the Coulomb-Attenuating Method (CAM-B3LYP). *Chem. Phys. Lett.* **2004**, *393*, 51-57.